Acta Crystallographica Section D
Biological Crystallography
ISSN 0907-4449

Structure of the insecticidal bacterial δ-endotoxin Cry3Bb1 of *Bacillus thuringiensis*

Nikolai Galitsky,[a] Vivian Cody,[a]* Andrzej Wojtczak,[b] Debashis Ghosh,[a,c] Joseph R. Luft,[a] Walter Pangborn[a] and Leigh English[d]†

[a]Hauptman–Woodward Research Institute, Inc., 73 High Street, Buffalo, NY 14203-1196, USA, [b]Faculty of Chemistry, N. Copernicus University, Gagarina 7, 87-100 Torun, Poland, [c]Roswell Park Cancer Research Institute, Buffalo, NY, USA, and [d]Ecogen Inc., 2005 Cabott Boulevard West, Langhorne, PA 19047-1810, USA

† Current address: Monsanto Company, 700 Chesterfield Parkway North, St Louis, MO 63198, USA.

Correspondence e-mail: cody@hwi.buffalo.edu

Received 14 December 2000
Accepted 15 May 2001

PDB Reference: δ-endotoxin Cry3Bb1, 1ji6.

The coleopteran-active δ-endotoxin Cry3Bb1 from *Bacillus thuringiensis* (Bt) strain EG7231 is uniquely toxic to *Diabrotica undecimpunctata*, the Southern corn rootworm, while retaining activity against *Leptinotarsa decemlineata*, the Colorado potato beetle. The crystal structure of the δ-endotoxin Cry3Bb1 has been refined using data collected to 2.4 Å resolution, with a residual R factor of 17.5% and an $R_{\rm free}$ of 25.3%. The structure is made up of three domains: I, a seven-helix bundle (residues 64–294); II, a three-sheet domain (residues 295–502); and III, a β-sandwich domain (residues 503–652). The monomers in the orthorhombic $C222_1$ crystal lattice form a dimeric quaternary structure across a crystallographic twofold axis, with a channel formed involving interactions between domains I and III. There are 23 hydrogen bonds between the two monomers conferring structural stability on the dimer. It has been demonstrated that Cry3Bb1 and the similar toxin Cry3A form oligomers in solution. The structural results presented here indicate that the interactions between domains I and III could be responsible for the initial higher order structure and have implications for the biological activity of these toxins. There are seven additional single amino-acid residues in the sequence of Cry3Bb1 compared with that of Cry3A; one in domain I, two in domain II and four in domain III, which also shows the largest conformational difference between the two proteins. These changes can be implicated in the selectivity differences noted for these two δ-endotoxins.

1. Introduction

B. thuringiensis (Bt) is a Gram-positive soil bacterium characterized in part by its ability to produce crystalline inclusions during sporulation. These inclusions consist of proteins exhibiting highly specific insecticidal activity which are referred to as δ-endotoxins or insecticidal crystal proteins. Most commercially important Bt strains express a variety of different δ-endotoxins selected for specific pest-control capabilities. The currently known *B. thuringiensis* δ-endotoxins have been grouped into 22 classes based on sequence homology (Crickmore *et al.*, 1998; Schnepf, 1995). The updated nomenclature and dendrogram of Bt δ-endotoxins can be found at http://www.biols.susx.ac.uk/home/Neil_Crickmore/Bt. The Cry3 class is best known for insecticidal activity against larval Coleoptera. Both Cry3A and Cry3Bb1 are EPA registered for use in biopesticides. Cry3A is also registered for use in transgenic plants.

The molecular weights of δ-endotoxins range from 135–140 kDa (Cry1 protoxins) to 55–72 kDa for activated Cry1,

Cry2 and Cry3 toxins. These toxins must be solubilized in the insect digestive tract and in some cases activated to smaller molecular-weight forms, *e.g.* Cry1 protoxin (135 kDa) to Cry1 (55 kDa) activated toxin (Bulla *et al.*, 1977). During activation, peptides are removed from both the N- and C-terminus of the protoxin. In solution, some toxins form quaternary structures (Walters *et al.*, 1994), a process that may be required for formation of even higher order polymeric structures in artificial bilayers to explain the extremely high conductances generated by these toxins (Slatin *et al.*, 1990). Analysis of data from polyacrylamide-gel and analytical ultracentrifugation experiments suggests that the size of the Cry3A oligomer in solution is a dimer. Structural data for Cry3A reveal that the toxin is made up of three domains (Li *et al.*, 1991) and that toxin monomers form a dimeric structure in the crystal lattice. Based on the equivalent migration on polyacrylamide gels of Cry3Bb1 and Cry3A, which have 85% sequence homology, it is assumed that the quaternary structure of Cry3Bb1 is also a dimer (Walters *et al.*, 1994; English, unpublished analytical ultracentrifugation data).

After solubilization, the toxins must bind to receptors on brush-border epithelia in the insect midgut, a combination stomach and small intestine. The receptor for Cry3 proteins has not been identified, although Cry3 proteins bind to brush-border membrane vesicles isolated from *Leptinatarsa decemlineata* (Slaney *et al.*, 1992; Belfiore *et al.*, 1994). A Bt toxin–receptor protein complex for Cry1Ac contained aminopeptidase N and alkaline phosphatase and has been successfully reconstituted (Sangadala *et al.*, 1994). This complex reduces the effective concentration of the toxin by at least 1000-fold, consistent with previous experiments with reconstituted brush border that also reduced the effective toxin concentration by 1000-fold (English *et al.*, 1991). In independent experiments (Knight *et al.*, 1994), aminopeptidase N was observed to be the primary binding protein for Cry1Ac and Cry1Aa in *Manduca sexta*. Another binding protein reported is a 210 kDa membrane glycoprotein that specifically binds the Cry1Ab toxin of Bt subspecies *berliner* (Vadlamudi *et al.*, 1995). This protein is different from the Cry1Ac receptor–protein complex containing aminopeptidase N reconstituted by Sangadala *et al.* (1994). More recently, other aminopeptidase N enzymes have been characterized and shown to be the putative receptors for activated Cry1 toxins (Luo *et al.*, 1996; Denolf *et al.*, 1997; Hua *et al.*, 1998; Cooper *et al.*, 1998). Data for Cry1Ac revealed a biphasic binding mechanism to aminopeptidase N, as *N*-acetylgalactosamine inhibited the initial association but not the high-affinity state (Carroll *et al.*, 1997), and further analysis suggests that there is a two-step mechanism by which Cry1Ac binds and permeabilizes the midgut membrane (Cooper *et al.*, 1998). Mutational analysis of domain III residues in Cry1Ac also indicated that the mutated residues play an important role in binding by recognition of the sugar on the putative receptor glucosaminopeptidase N (Burton *et al.*, 1999).

Binding of δ-endotoxins to specific receptors effectively concentrates the toxin on the brush border, a process that probably also enhances the ability of the toxin molecules to associate together and spontaneously penetrate the bilayer. After assuming a membrane-bound position, the toxin forms ion channels that probably depend on the quaternary structure of the toxin and higher order structures that may form in the membrane (Slatin *et al.*, 1990). Eventually, large less specific pores 10–20 Å in diameter are formed by Bt toxins and colloid osmotic lysis kills the cell as demonstrated in insect-cell culture (Knowles & Ellar, 1987; Knowles *et al.*, 1991). The ion channels formed by δ-endotoxins are highly diverse. Cry1Ac and Cry3A form cation-selective and voltage-independent channels (Slatin *et al.*, 1990), while Cry2A and Cry3Bb1 form less selective but voltage-dependent channels (English *et al.*, 1994; Von Tersch *et al.*, 1994). It has also been reported that Cry1C forms pH-dependent anion-selective channels (Schwartz *et al.*, 1993, 1997).

Cry3Bb1 is a rootworm-active δ-endotoxin (Rupar *et al.*, 1991; Donovan *et al.*, 1992). The specific toxicity of Cry3Bb1 on the southern corn rootworm (*Diabrotica undecimpunctata*) suggests that differences in one or more of the steps in the mode of action create a uniquely toxic environment for Cry3Bb1 in the southern corn rootworm that is not achieved by Cry3A. Differences in solubility, oligomerization, binding and channel formation have been observed between Cry3Bb1 and other Cry3 toxins and these properties might all contribute to the unique insecticidal activity of this toxin (English, unpublished work).

To date, structural data are available only for coleopteran-specific Cry3A (Li *et al.*, 1991), the lepidopteran-specific Cry1Aa (Grochulski *et al.*, 1995) and the dipteran-specific protoxin CytB (Li *et al.*, 1996) from *B. thuringiensis*. Both Cry3A and Cry1Aa structures have three distinct domains and similar folds; however, there are significant differences in domain II of these toxins. The protoxin CytB has a single domain in an α/β dimer (Li *et al.*, 1996). We report the crystal structure determination at 2.4 Å resolution of Cry3Bb1, the structure of the coleopteran-active δ-endotoxin from *B. thuringiensis* (Bt) strain EG7231, and compare its structure with the homologous Cry3A and Cry1Aa endotoxins.

2. Materials and methods

As previously reported (Cody *et al.*, 1992; Galitsky *et al.*, 1994), crystals of Cry3Bb1 belong to the space group $C222_1$, with unit-cell parameters a = 122.44, b = 131.81, c = 105.37 Å, and contain one molecule in the asymmetric unit. Native data to 2.4 Å resolution and derivative data sets for Hg and Pt derivatives were collected at room temperature on a Rigaku R-AXIS IIc imaging-plate system (Table 1). Native crystals were soaked with heavy atoms for a period of 24–48 h. The structure of Cry3Bb1 was solved using multiple isomorphous replacement methods and the structure refined prior to the availability of the coordinates for Cry3A. Comparison of these two structures shows an overall r.m.s. for all backbone atoms of 1.6 Å with an average deviation of 0.8 Å for domain I, 0.7 Å for domain II and 1.3 Å for domain III, confirming the structure solution.

Heavy-atom sites in each derivative were located from difference Patterson functions using the program *HASSP* (Terwilliger & Eisenberg, 1983) and heavy-atom parameters were refined using the program *HEAVY* (Terwilliger & Eisenberg, 1983). Solvent-flattened data were prepared using the program of Wang (1985). The choice of enantiomorph was determined from the handedness of the α-helices. A single site for the Hg derivative and one major and five minor sites for the Pt data (Table 1) were used to phase the native data and produced interpretable electron-density maps. A continuous polypeptide chain from residues 64–652 was traced. The initial atomic model was built using the program *FRODO* (Jones, 1978) operating on a PS390 Evans and Southerland graphics system running on a VAX 8600 computer. Later refinement and model building were carried out using *X-PLOR* (Brünger, 1992) and *CHAIN* (Sack, 1988) running on a Silicon Graphics R10000. Refinement of the model by simulated annealing in *X-PLOR* (Brünger, 1992) reduced the *R* factor from 31.6 to 26.1% without individual *B* factors for 15 811 data in the resolution range 8–3 Å and to 22.1% for 26 236 data in the resolution range 8–2.5 Å with restrained individual *B* factors. Prior to refinement, 10% of the data, chosen at random with the protocol in *X-PLOR*, were selected to calculate $R_{\rm free}$. The model was adjusted between refinement cycles on the graphics and 251 water molecules were added in the final cycles of refinement. The final refinement parameters are shown in Table 2. A Ramachandran plot (Laskowski *et al.*, 1993) revealed that more than 92% of the residues were in their most favored conformations.

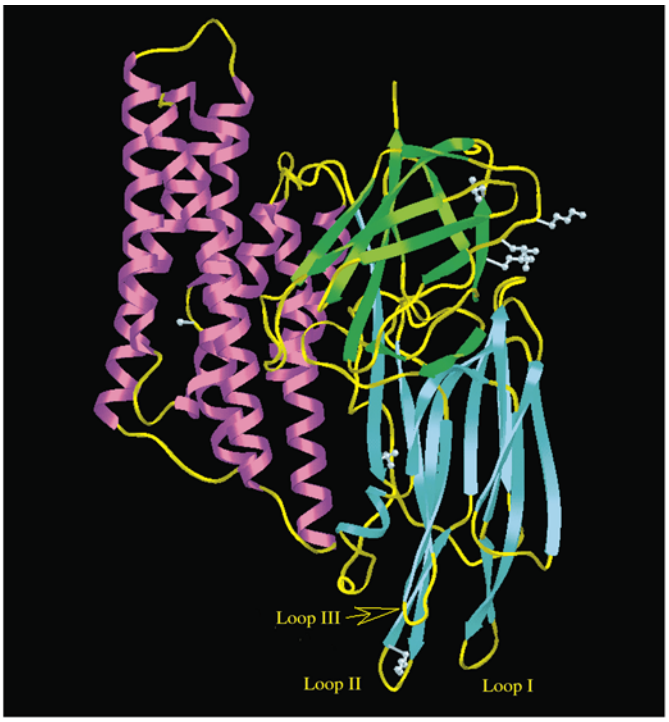

(*a*)

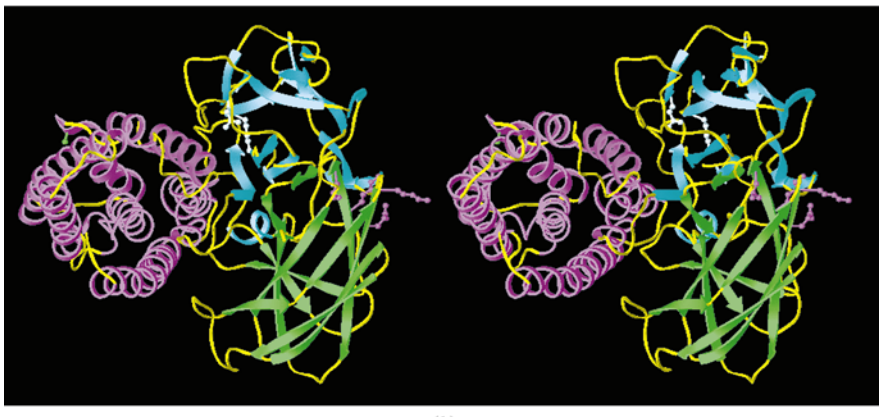

(*b*)

Figure 1
(*a*) Schematic ribbon representation of Cry3Bb1 showing its three-domain organization: domain I (magenta), domain II (cyan) and domain III (green). Loop connections are yellow. The sites of amino-acid insertion in this structure compared with Cry3A are shown in white (domain I, Ala104; domain II, Lys416, Gln453; domain III, Lys554, Leu557, Lys624, Glu626). Diagrams were produced with the program *SETOR* (Evans, 1993). (*b*). Stereo representation showing an alternate view of Cry3Bb1 highlighting the orientation of the seven-helical bundle of domain I.

3. Results

3.1. Tertiary structure

The structure of Cry3Bb1 is similar to Cry3A (Li *et al.*, 1991) and Cry1Aa (Grochulski *et al.*, 1995) and also has three discrete domains. In Cry3Bb1, domain I (residues 64–294) has a seven-helix bundle which forms a left-handed superhelix around a central helix, domain II (residues 295–503) has three antiparallel β-sheets and domain III (residues 504–652) has a sandwich structure with two antiparallel β-sheets (Fig. 1). Similar to Cry3A (Li *et al.*, 1991), the first 60 N-terminal residues of Cry3Bb1 were also not observed in this crystal structure. There are seven additional single amino acids (*i.e.* Ala104, Lys416, Gln453, Lys554, Leu557, Lys624 and Glu626) in the sequence of Cry3Bb1 compared with that of Cry3A. The majority of these insertions are located in domain III. As expected because of the high degree of sequence homology, the two structures have similar conformations, with the largest differences observed in domain III.

The seven-helical bundle of domain I is long and twisted around the central helix α5 surrounded by six outer helices, which creates greater structural stability for the bundle (Fig. 1). The outer helices are oriented counterclockwise when viewed from the C- to the N-terminus around the central helix, with helices α1 and α7 adjacent to the β-sheet domains (Fig. 2). The residues which make up the helical bundle encompass residues 64–80 for helix α1, 91–99 for helix α2a, 106–118 for helix α2b, 123–154 for helix α3, 160–187 for helix α4, 197–215 for helix α5, 223–255 for helix α6 and 259–284 for helix α7. Helix α2 is interrupted by a non-

Table 1
Data-collection and phasing statistics for Cry3Bb1.

	Native	K_2PtCl_4	$HgCl_2$
Unit-cell parameters (Å)			
a	122.44	121.75	121.32
b	131.81	132.00	131.99
c	105.37	105.52	105.92
Detector	R-AXIS IIc		
Temperature (K)	293	293	293
Heavy-atom conc. (m*M*)		10	100
Soaking time (h)		48	40
No. of reflections			
Total	91281	47734	44793
Unique	30077	15638	14678
Resolution (Å)	2.40	2.80	2.80
Completeness (%)	72.2		
R_{merge}	7.66	10.92	9.46
Number of sites		1	1 major, 5 minor
Phasing power†		1.99	2.16

† Phasing power = $\langle F_H \rangle$, r.m.s. heavy-atom *F* divided by residual lack of closure.

Table 2
Refinement statistics for Cry3Bb1.

Unit-cell parameters (Å)	122.44, 131.81, 105.4
Space group	$C222_1$
Resolution range (Å)	8.0–2.4
Reflections used	27379
Reflections in test set	3049
R factor (%)	17.5
R_{free} (%)	25.3
Average *B* factor	30.22
Protein atoms	4750
Water molecules	251
Bond-length deviation (Å)	0.009
Bond-angle deviation (°)	1.30
Ramachandran plot	
Residues in most favored region (%)	92.1
Residues in additional allowed region (%)	8.9

helical segment between residues 100–105 and includes an additional residue, Ala104, compared with the sequence of Cry3A (Li *et al.*, 1991) (Figs. 3 and 4). There is greater surface exposure of residues Ser102 and Asp103 in Cry3Bb1 as a result of this insertion. The major changes in domain I of these two toxins involve the conformation of loop regions encompassing residues 81–90, 100–105, 155–159 and 216–222. Also, three more N-terminal residues were observed in the tertiary structure of Cry3A than in Cry3Bb1.

Of the two α2 helical segments, only helix α2b is packed against helix α5. The other helices are long and, similar to the structure reported for Cry3A (Li *et al.*, 1991), have eight, seven, six, nine and seven helical turns in helices α3–α7, respectively. There are two γ-turns in the loop between helix α4 and α5. The loop between helix α6 and α7 is close to the loop region for residues 310–318 of domain II, which has contacts of 2.9 Å between the side chains of residues Asp261 and Gln316.

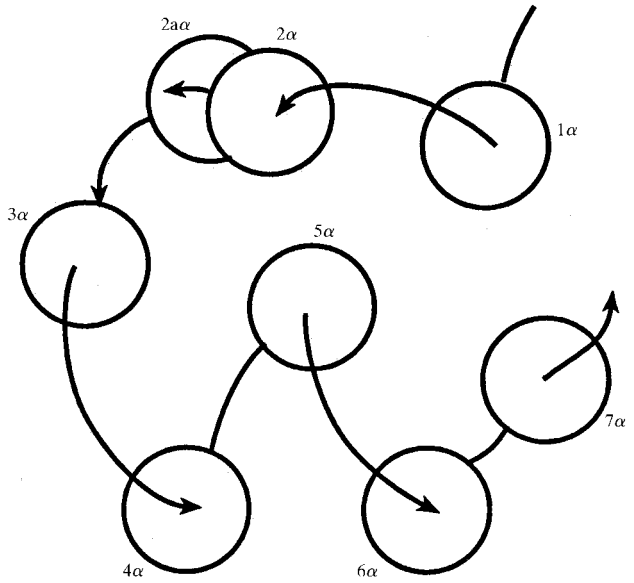

Figure 2
Projection of the seven-helix bundle of domain I with helices represented as circles, similar to the orientation of domain I in Fig. 1(*b*).

In domain I, helices α6 and α7 are packed further away from the other helices in the bundle. The loops at the bottom of these helices also lie near loop 310–318 of domain II and form a series of close interactions involving Ser258 O···Phe322 N (2.8 Å), Asp261 OD1···Gln31 NE26 (2.9 Å), Asn267 ND2···Phe305 O (3.0 Å), and a salt bridge between Arg270 NH1···Glu326 OE1 (2.9 Å) and Arg270 NH2···Glu326 OE2 (3.3 Å). There is also an interaction with water (Arg270 NH2···Wat68 O, 2.7 Å). In addition, Glu326 interacts with Trp263 (Trp263 NE1···Glu326 OE1, 3.0 Å).

Domain II (Fig. 5; residues 295–501) contains three antiparallel β-sheets. Sheet 1, composed of strands β5, β2, β3 and β4, and sheet 2, composed of strands β8, β7, β6 and β9, form the distinctive 'Greek key' motif, similar to that observed in Cry3A (Li *et al.*, 1991). The outer surface of sheet 3 (β1, β11 and β10) makes contact with helix α7 of domain I. There is also a pocket formed by part of helix α6 and α7 and the loop of strands β1 and β2 of domain II. The strand which begins at residue 295 follows the face of domain I to the loop at residues 310–318, which along with the loop at residues 350–355, acts as a hook projecting out of the surface of domain II and interacts with the loop between helices α6 and α7. Interactions between domains I and II are strengthened by a hydrogen bond between Gln316 of domain II and Asp261 of domain I. This interaction is not observed in the structure of Cry3A owing to changes in the local conformation as a consequence of the differences in the sequence of these two proteins. Comparison of the loop conformation of residues 310–318 of Cry3Bb1 and the corresponding regions of Cry3A (Li *et al.*, 1991) and Cry1Aa (Grochulski *et al.*, 1995) show differences that suggest this region is flexible (Fig. 5). The contacts between domains I, II and III form a cavity filled with waters which hydrogen bond among themselves and the adjacent protein side chains.

There are two additional residues in domain II of Cry3Bb1 not present in the sequence of Cry3A: Lys416 and Gln453. A

possible effect of the insertion of Lys416 in domain II is to stabilize the structure by formation of a hydrogen bond to Asp486 (2.9 Å) and thereby stabilize the conformation of the two loops between residues 310–318 and residues 485–488. Additionally, the side chain of Arg487 is extended and is oriented in the same direction as Lys416, thereby forming a hydrophilic pocket surrounded by residues Lys416, Tyr418, Asp486 and Arg487 (Fig. 6). This stability is not present in Cry3A as there are no equivalent side chains capable of hydrogen-bond formation (Cry3A has a glycine in position 486). Thus, without this additional residue found in Cry3Bb1, the side chains of Cry3A are not close enough to form hydrogen-bond contacts.

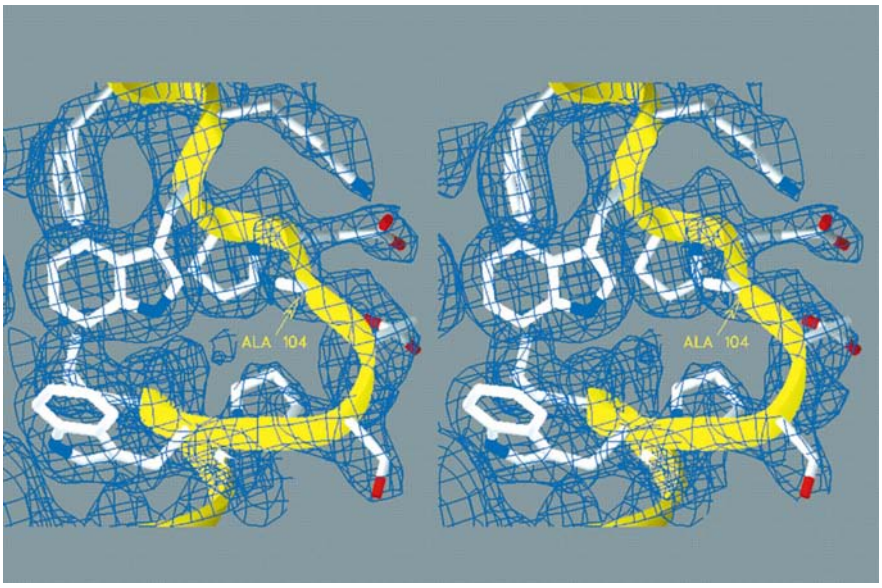

Figure 3
Stereo electron-density profile ($2F_o - F_c$, 1σ) for region in domain I of Cry3Bb1 showing the insertion of Ala104. Backbone ribbon (yellow) and side chains (white) in the loop region are shown.

The insertion of Gln453 in Cry3Bb1 (Fig. 7) terminates the loop region between residues 443 and 453 which deviates in conformation from the loop observed in the structure of Cry3A (Li *et al.*, 1991). As a result, Gln453 participates in hydrogen bonds with the backbone of Asp307 and a water molecule, which in turn hydrogen bonds to the hydroxyl group of Thr403. In the structure of Cry3A, Trp450 occupies the same space as Gln453 and forms a hydrogen bond with the backbone of residue Thr306, but cannot form the hydrogen bond through water, as Ala401 has no hydrogen-bond acceptor.

The most significant differences between the tertiary structure of Cry3Bb1 and that reported for Cry3A are in domain III (residues 503–652) (Fig. 8), which has a 'jelly-roll' β-barrel topology with a hydrophobic core, whereas domain III of Cry1Aa has the greatest similarity to domain III of Cry3A (Grochulski *et al.*, 1995). There are four single-residue insertions in domain III of Cry3Bb1 (*i.e.* Lys554, Leu557, Lys624 and Glu626) not present in the sequence of Cry3A (Li *et al.*, 1991). As shown (Fig. 8), these residues all lie on one surface of domain III between strands $\beta16$–$\beta17$ and $\beta22$–$\beta23$. The two single-residue insertions at positions 554 and 557 form an α-turn and the two-residue insertion at positions 624 and 626 of loop 622–625 causes it to extend, finger-like, from the surface of domain III. The side chain of the inserted residue Glu626 forms a hydrogen bond to Tyr521 (2.8 Å) and provides more structure for the turn around loop residues 620–625 by formation of hydrogen bonds Asn625 ND2···Ser621 O (2.9 Å) and Asn625 ND2···Gly622 O (2.7 Å).

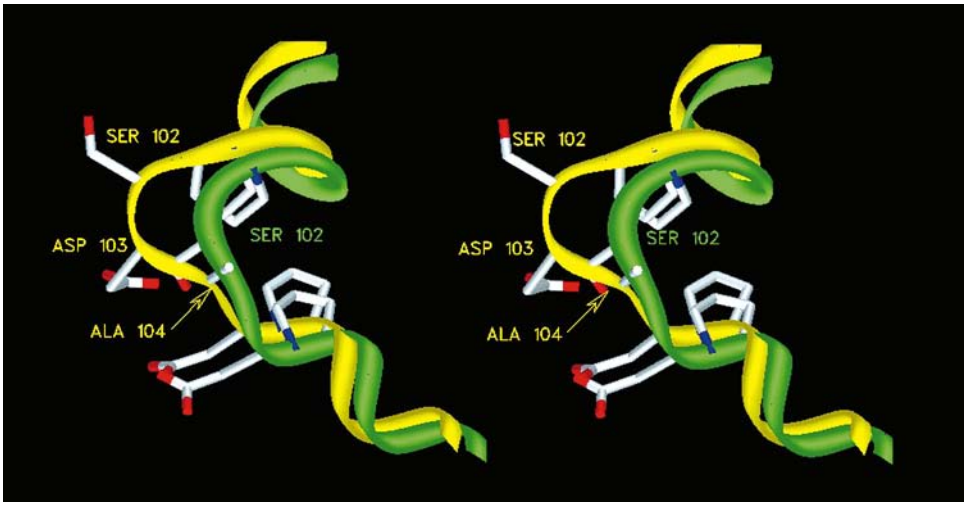

Figure 4
Comparison of the region encompassing the insertion at position 104 of Cry3Bb1 (yellow) and Cry3A (green). Note that residues 102 and 103 (white) have more surface exposure as a result of this insertion.

3.2. Quaternary association

Crystal packing along the twofold axis parallel to the *a* axis results in a dimer of Cry3Bb1 (Fig. 9), which also reveals the interaction between helices $\alpha3$ and $\alpha4$ of two molecules related along the twofold axis. This is also a feature of the packing in the structure of Cry3A (Li *et al.*, 1991), but is not the case in the structure of Cry1Aa (Grochulski *et al.*, 1995). Helix $\alpha6$ lies in a cleft formed by the interface of domain I, its symmetry-related molecule and domain III. There are 23 close hydrogen-bonding contacts along this pocket surface, 11 contributed from each

monomer and one intramolecular hydrogen bond involving His231 NE2···Tyr230 OH. Solvent is also present in this cleft, which participates in two additional hydrogen bonds between the two monomers. Along this surface there is another cleft formed near residue His231 which is near the top of helix α6 of domain I. There are three water molecules in the cleft, which form a network of hydrogen bonds involving the side chains of His231 NE2···
Tyr230 OH (2.9 Å) from two symmetry-related molecules and, within the same molecule, His231 NE2···Asp288 OD1 (2.9 Å), Wat13 O···Tyr606 OH (2.9 Å), Wat48 O···Asp288 OD1 (2.6 Å) and Wat48 O···Wat13 O (2.7 Å). Similar interactions are also observed along the dimer interface in the structure Cry3A; however, a sequence change from His231 to Lys230 in Cry3A results in fewer hydrogen-bond interactions.

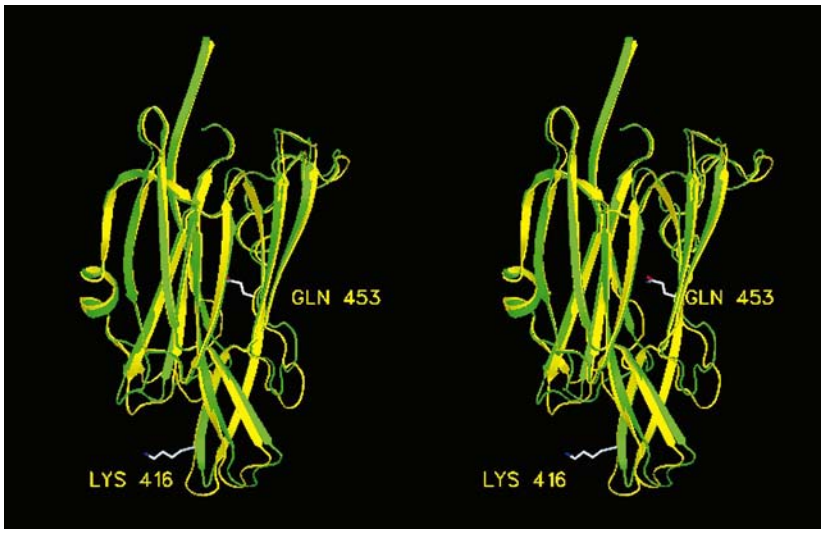

Figure 5
Comparison of domain II for Cry3Bb1 (yellow) and Cry3A (green), illustrating the three antiparallel β-sheets. The sites of amino-acid insertion, residues Lys416 and Gln453, are also highlighted.

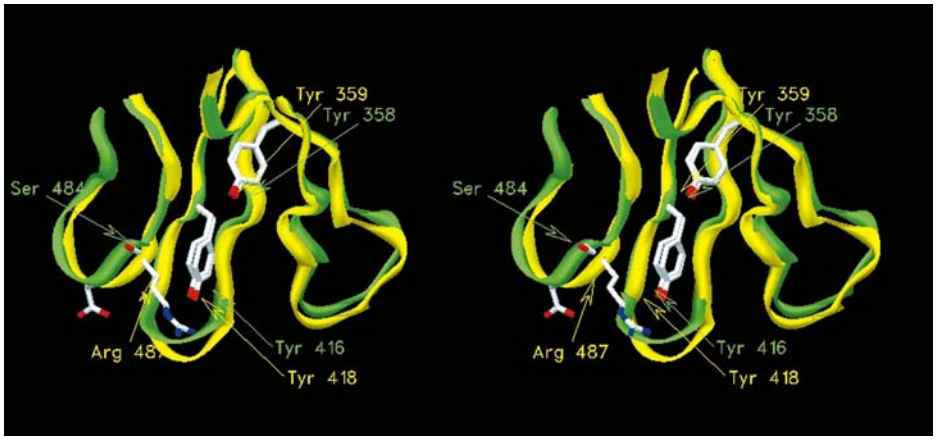

Figure 6
Comparison of the region near the insertion of residue Lys416 in Cry3Bb1 (yellow) with Cry3A (green). This residue points to a hydrophilic pocket with conserved tyrosyl groups.

4. Discussion

4.1. Functional role of domains

Since the publication of the Cry3A structure, researchers have been able to assign some functions to particular toxin structures. It has been demonstrated that only the α-helical bundle of Cry3Bb1 (Von Tersch *et al.*, 1994) and domain I of Cry1Ac, also presumed to be an α-helical bundle, are capable of forming ion channels (Walters *et al.*, 1994; Chen *et al.*, 1993) confirming the suggestion from the crystal structure that this is a membrane-active region (Li *et al.*, 1991). Helix α5 has been specifically implicated in the channel-formation process (Gazit & Shai, 1993, 1995; Gazit *et al.*, 1994, 1998), as a slightly modified synthetic helix α5 is highly membrane active. These data suggest that only domain I or a portion of domain I need penetrate the membrane to account for the ion-channel activity of δ-endotoxins, although the mechanism whereby these channel-forming toxins and toxin fragments are able to assume a membrane-bound form and produce the structure capable of forming channels has not yet been determined.

One of the processes that might lead to the formation of the membrane-bound toxin is the ability of the toxin to form oligomeric structures. Cry3A and Cry3Bb1 both oligomerize in solution (Walters *et al.*, 1994), but this process may continue even further in the membrane. Additional evidence for a dimer structure in solution for Cry3Bb1 is apparent from the crystal structure, which reveals extensive hydrogen bonding across the domain I–domain III interface. Thus, the function of domain III could include the propensity to form an oligomer in solution and thereby increase the stability of the protein. While it is tempting to propose that the ion channel is formed at the dimer interface, the question about the membrane-bound structure really must be resolved before an accurate proposal for the ion-channel structure is made. Nonetheless, the assignment of a discrete solution quaternary structure for a δ-endotoxin provides a starting point for determining events that may subsequently occur at the membrane.

Analysis of the ion channels formed by full-length Cry3Bb1 and domain I alone suggest that the channel characteristics of domain I might be modulated by other domains (Von Tersch *et al.*, 1994). Differences between domain I from Cry1Ac and the activated toxin were also reported (Walters *et al.*, 1993). The differences in domain III

between the two Cry3 structures may be important in forming dimers and the probability of forming higher order structures in the membrane. Chen *et al.* (1993) demonstrated that the arginine-rich β-strand (β22) can dramatically alter the behavior of the ion channels produced by Cry1Aa. It is notable that β-22 in Cry3Bb1 rests alongside domain I and is theoretically in a position to modulate the behavior of the toxin-formed ion channels. Schwartz (2000) suggests that a tetrameric form of Cry1Ac exists in the membrane. The forces that hold this oligomer together in the membrane are not known and may not be the same as the interactions observed between domain III and domain I in the Cry3Bb1 homodimer.

The prominent loop regions of domain II in Cry3A have been implicated in the binding of the toxin to the brush-border epithelium of the insect midgut membrane. These same loop regions are a prominent feature of Cry3Bb1 and by analogy may play a critical role in binding and insecticidal specificity. Care must be taken, however, in the assignment of the binding function to domain II only. Mutations in domain I from Cry1A toxins dramatically alter the binding properties of these toxins (Wu & Aronson, 1992). These data suggest that both domain I and domain II participate in the binding function. Chen *et al.* (1995), for example, also demonstrated that alterations in domain I of Cry1Ab altered the binding properties of this toxin. In addition, the formation of a stable dimer (involving domain III) may also be important to effective receptor–toxin interactions. Mutagenic studies of the surface loops in domain II of Cry3A suggest that loop III (residues 481–486) may play a role in membrane insertion (Wu & Dean, 1996). Structural data for Cry1Aa and Cry3A reveal that these loops are highly mobile, as reflected by their higher thermal motion and support these mutational data. Similar mutational studies in these loop regions of domain II of Cry1C reveal that changes in these regions can selectively affect toxicity for different species (Abdul-Raul & Ellar, 1999).

Li *et al.* (1991) suggested that one function of domain III was to provide proteolytic stability to the toxin. While this may be true, to date no confirmation of this hypothesis has been obtained. From the analysis of the quaternary structure of Cry3Bb1, an additional argument can also be made for the involvement of domain III in the formation of a stable dimer in solution. Thus, the function of domain III should include the propensity to form a solution oligomer. Assignment of segregated functions to each of the three domains has provided significant experimental ideas, but the data suggest that functions and domains are probably not strictly segregated (English *et al.*, 1995).

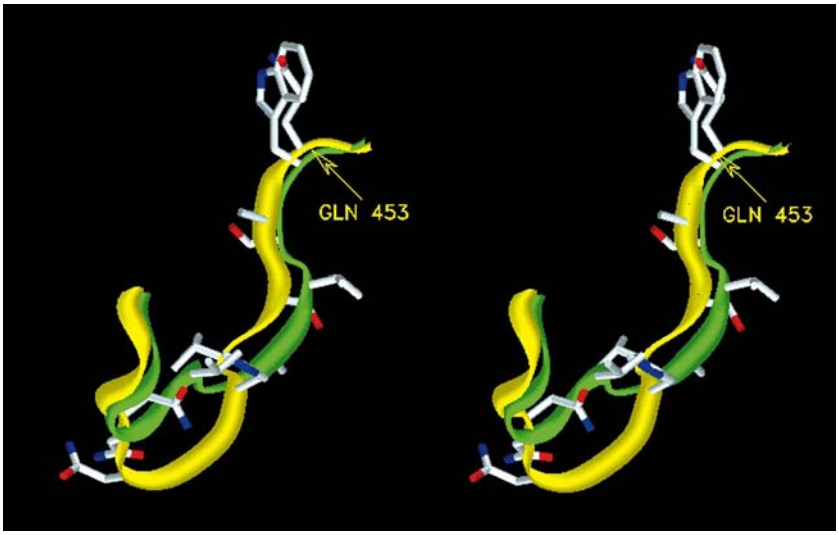

Figure 7
Comparison of Cry3Bb1 (yellow) and Cry3A (green) showing conformational differences influenced by the insertion of Gln453.

Bt toxins have in part a common pore-forming function with other bacterial toxins, *e.g.* colicins, diphtheria toxin and staphlococcus α toxin (Ghosh *et al.*, 1994; Qiu *et al.*, 1995), but the structural information presented here does not permit extrapolation to a common mechanism of pore formation. It is reasonable to suggest, however, that like other bacterial toxins some structural rearrangements occur upon membrane association (Parker *et al.*, 1989; Slatin *et al.*, 1994). In the case of colicin Ia (Parker *et al.*, 1989) and diphtheria toxin (Slatin *et al.*, 1994; Silverman *et al.*, 1994), only a part of the α-helical bundle needs to penetrate the membrane for full ion-channel activity. Gazit & Shai (1995) have demonstrated that helix 5 is a channel-forming helix and that helix 7 may also participate in the membrane activity of Cry3A. Caution, however must be taken in extrapolating from this research, as helix 5 is one tenth as active a pore former as the full-length toxin.

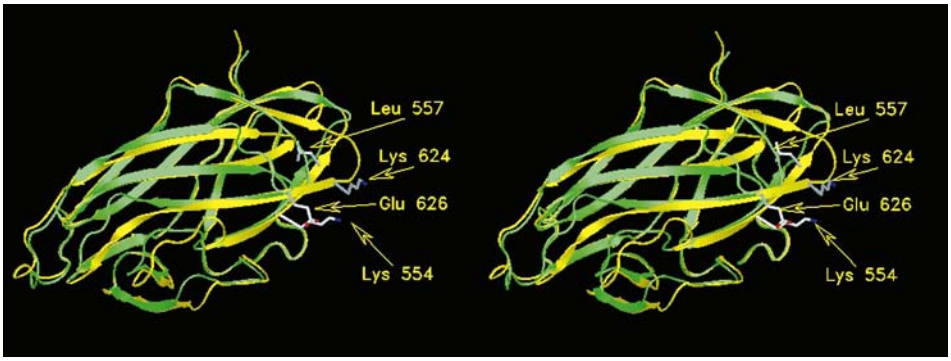

Figure 8
Comparison of domain III for Cry3Bb1 (yellow) and Cry3A (green), illustrating the 'jelly-roll' β-barrel topology. Positions 554, 557, 624 and 626 are additional residues in Cry3Bb1 not present in Cry3A. Note that the additional residues all lie on one surface of domain III.

5. Summary

We report the crystal structure of Cry3Bb1 from the Bt strain EG7231 refined to 2.4 Å resolution. These data reveal that the structure of Cry3Bb1 is made up of three domains, similar to that observed for the structure of Cry3A, with which Cry3Bb1 shares 85% sequence homology. There are seven single-residue insertions in the sequence of Cry3Bb1 compared with that of Cry3A. Domain I has a seven-helical bundle with a central α-helix, domain II is composed of three antiparallel β-sheets and domain III has a sandwich structure with two antiparallel β-sheets. The monomers in the crystal form a dimeric quaternary structure across a crystallographic twofold axis, with a solvent pocket formed involving interactions between domains I and III.

It has been demonstrated recently that only the α-helical bundle of domain I of Cry3Bb1 is sufficient to form ion channels. These data suggest that domain I penetrates the membrane to account for the ion-channel activity. One process that might lead to the formation of membrane-bound toxins is the ability to form higher order structures. Thus, the observation of dimer formation in the crystal structure of Cry3Bb1 supports this hypothesis. Also, differences in domain III between the structure of Cry3Bb1 and Cry3A may be important in the regulation of channel function at the dimer interface, as well as imparting specificity of action.

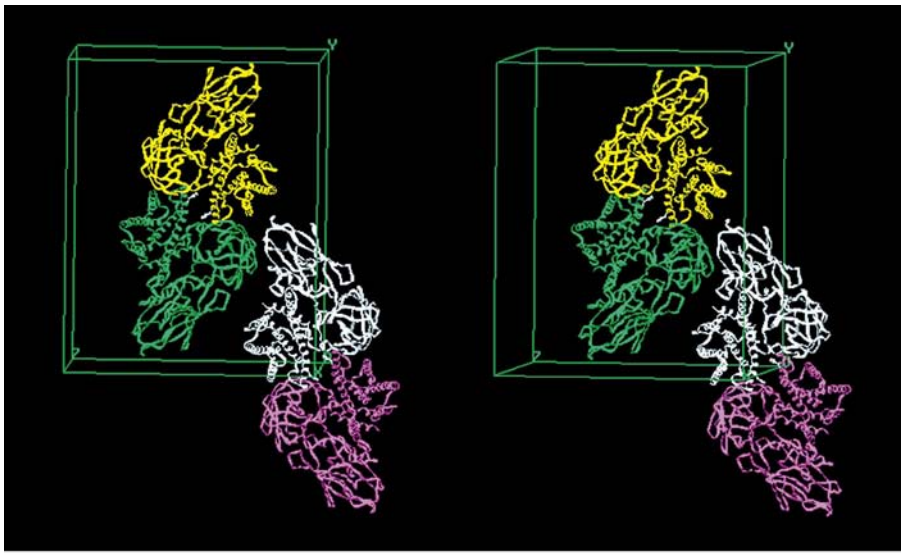

(*a*)

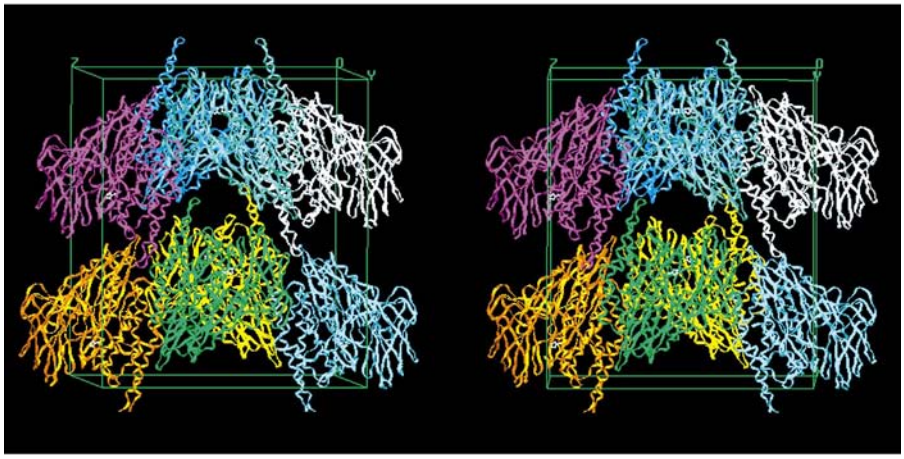

(*b*)

Figure 9
(*a*) Stereo crystal packing of Cry3Bb1 in space group $C222_1$ projected down the twofold axis along the x axis, highlighting the dimer arrangement between pairs of molecules shown for one layer of packing. Also illustrated is the side chain of His231 (white). Color assignment not the same as in (*b*). (*b*) Stereo diagram of the full crystal packing in space group $C222_1$ viewed along the y axis, illustrating a solvent channel. The molecules are colored by symmetry operator: x, y, z, white; $-x$, $-y$, $\frac{1}{2}+z$, yellow; x, $-y$, $-z$, violet; $\frac{1}{2}+x$, $\frac{1}{2}+y$, z, cyan; $\frac{1}{2}-x$, $\frac{1}{2}-y$, $\frac{1}{2}+z$, blue; $\frac{1}{2}-x$, $\frac{1}{2}+y$, $\frac{1}{2}-z$, pale green; $\frac{1}{2}+x$, $\frac{1}{2}-y$, $-z$, gold.

The authors thank C. Kulesza and A. Bastian for their help in the preparation and purification of the Cry3Bb1 samples, M. Von Tersch for preparing *B. thuringiensis* and *B. megaterium* cultures expressing Cry3Bb1, and W. Donovan for the use of EG7231 for the production of Cry3Bb1. We also thank Drs Charles M. Weeks and Zdzislaw Wawrzak for their help with the heavy-atom phasing and protocols for *X-PLOR* refinement.

References

Abdul-Raul, M. & Ellar, D. J. (1999). *Curr. Microbiol.* **39**, 94–98.
Belfiore, C. J., Vadlamudi, R. K., Osman, Y. A. & Bulla, L. A. (1994). *Biochem. Biophys. Res. Commun.* **200**, 359–364.
Brünger, A. T. (1992). *X-PLOR Manual Version* 3.1. Yale University Press, New Haven, CT, USA.
Bulla, L. A., Kramer, K. J. & Davidson, L. I. (1977). *J. Bacteriol.* **130**, 375–383.
Burton, S. L., Ellar, D. J., Li, J. & Derbyshire, D. J. (1999). *J. Mol. Biol.* **287**, 1011–1022.
Carroll, J., Wolfersberger, M. G. & Ellar, D. J. (1997). *J. Cell Sci.* **110**, 3099–3104.
Chen, X.-J., Curtiss, A., Alcantara, E. & Dean, D. H. (1995). *J. Biol. Chem.* **270**, 6412–6419.
Chen, X.-J., Lee, M. K. & Dean, D. H. (1993). *Proc. Natl Acad. Sci. USA*, **90**, 9041–9045.
Cody, V., Luft, J. R., Jensen, E., Pangborn, W. & English, L. (1992). *Proteins Struct. Funct. Genet.* **14**, 324.
Cooper, M. A., Carroll, J., Travis, E. R., Williams, D. H. & Ellar, D. J. (1998). *Biochem. J.* **333**, 677–683.
Crickmore, N., Zeigler, D. R., Feitelson, J., Schnepf, E., Van Rie, J., Lereclus, D., Baum, J. & Dean, D. H. (1998). *Microbiol. Mol. Biol. Rev.* **62**, 807–813.
Denolf, P., Hendrickx, K., Van Damme, J., Jansens, S., Peferoen, M., Degheele, D. & Van Rie, J. (1997). *Eur. J. Biochem.* **248**, 748–761.

Donovan, W. P., Rupar, M. J., Slaney, A. C., Malvar, T., Gawron-Burke, M. C. & Johnson, T. B. (1992). *Appl. Environ. Microbiol.* **58**, 3921–3927.
English, L. H., Readdy, T. L. & Bastian, A. E. (1991). *Insect Biochem.* **21**, 177–184.
English, L. H., Robbins, H. L., Von Tersch, M. A., Kulesza, C. A., Ave, D., Coyle, D., Jany, C. S. & Slatin, S. L. (1994). *J. Insect. Biochem. Mol. Biol.* **24**, 1025–1035.
English, L. H., Walters, F., Von Tersch, M. A. & Slatin, S. (1995). *Molecular Action of Insecticides in Ion Channels*, edited by J. M. Clark, *American Chemical Society Symposium Series* 591, pp. 302–307. Washington DC: American Chemical Society
Evans, S. V. (1993). *J. Mol. Graph.* **11**, 134–138.
Galitsky, N., Cody, V., Wojtczak, A., Ghosh, D., Wawrzak, Z., Luft, J. R., Pangborn, W. & English, L. (1994). Am. Crystallogr. Assoc. Meet. Abstract No. PTX10, p. 180.
Gazit, E., Bach, D., Kerr, I. D., Sansom, M. S. P., Chejanovsky, N. & Shai, Y. (1994). *Biochem. J.* **304**, 895–902.
Gazit, E., La Rocca, P., Sansom, M. S. & Shai, Y. (1998). *Proc. Natl Acad. Sci. USA*, **95**, 12289–12294.
Gazit, E. & Shai, Y. (1993). *Biochemistry*, **32**, 3429–3436.
Gazit, E. & Shai, Y. (1995). *J. Biol. Chem.* **270**, 2571–2578.
Ghosh, P., Mel, S. F. & Stroud, R. M. (1994). *Struct. Biol.* **1**, 597–604.
Grochulski, P., Masson, L., Borisova, S., Pusztai-Carey, M., Schwartz, J. L., Brousseau, R. & Cygler, M. (1995). *J. Mol. Biol.* **254**, 447–464.
Hua, G., Tsukamoto, K. & Ikezawa, H. (1998). *Comput. Biochem. Physiol. B*, **121**, 213–222.
Jones, T. A. (1978). *J. Appl. Cryst.* **11**, 268–272.
Knight, P. J. K., Crickmore, N. & Ellar, D. J. (1994). *Mol. Microbiol.* **11**, 429- 436.
Knowles, B. H. & Ellar, D. J. (1987). *Biochem. Biophys. Acta*, **924**, 509–518.
Knowles, B. H., Knight, P. K. & Ellar, D. J. (1991). *Proc. R. Soc. London Ser. B*, **245**, 31–35.
Laskowski, R. A., MacArthur, M. W., Moss, D. S. & Thornton, J. M. (1993). *J. Appl. Cryst.* **26**, 283–291.
Li, J., Carroll, J. & Ellar, D. J. (1991). *Nature (London)*, **353**, 815–821.
Li, J., Koni, P. A. & Ellar, D. J. (1996). *J. Mol. Biol.* **257**, 129–152.
Luo, K., Lu, Y.-J. & Adang, M. J. (1996). *Biochem. Mol. Biol.* **26**, 783–791.
Parker, M. W., Pattus, F., Tucker, A. D. & Tsernoglou, D. (1989). *Nature (London)*, **337**, 93–96.
Qiu, X., Verlinde, C. L. M. J., Zhang, S., Schmitt, M. P., Holmes, R. K. & Hol, W. G. J. (1995). *Structure*, **3**, 87–100.
Rupar, M. J., Donovan, W. P., Groat, R. G., Slaney, A. C., Mattison, J. W., Johnson, T. B., Charles, J.-F., Dumanoir, V. C. & de Barjac, H. (1991). *Appl. Environ. Microbiol.* **57**, 3337–3344.
Sack, J. (1988). *J. Mol. Graph.* **6**, 244–245.
Sangadala, S., Walters, F. S., English, L. H. & Adang, M. J. (1994). *J. Biol. Chem.* **269**, 10088–10092.
Schnepf, H. E. (1995). *Curr. Opin. Biotechnol.* **6**, 305–312.
Schwartz, J. L. (2000). *Abstracts of the Ion Channels Meeting, Trento, Italy*, p. 46.
Schwartz, J. L., Garneau, L., Savaria, D., Masson, L., Brousseau, R. & Rousseau, E. (1993). *J. Membr. Biol.* **132**, 53–62.
Schwartz, J. L., Lu, Y.-J., Sohnlein, P., Brousseau, R., Laprade, R., Masson, L. & Adang, M. J. (1997). *FEBS Lett.* **412**, 270–276.
Silverman, J. A., Mindell, J. A., Zhan, H., Finkelstein, A. & Collier, R. J. (1994). *J. Membr. Biol.* **137**, 17–28.
Slaney, A. C., Robbins, H. L. & English, L. H. (1992). *Insect Biochem. Mol. Biol.* **22**, 9–18.
Slatin, S. L., Abrams, C. K. & English, L. (1990). *Biochem. Biophys. Res. Commun.* **169**, 765–772.
Slatin, S. L., Qui, X.-Q., Jakes, K. S. & Finkelstein, A. (1994). *Nature (London)*, **371**, 158–161.
Terwilliger, T. C. & Eisenberg, D. (1983). *Acta Cryst.* A**39**, 813–817.
Vadlamudi, R. T., Weber, E., Ji, I., Ji, T. H. & Bulla, L. A. (1995). *J. Biol. Chem.* **270**, 5490–5495.
Von Tersch, M. A., Slatin, S. L., Kulesza, C. A. & English, L. H. (1994). *Appl. Env. Microbiol.* **60**, 3711–3717.
Walters, F. S., Kulesza, C. A., Philips, A. T. & English, L. H. (1994). *Insect Biochem. Mol. Biol.* **24**, 963–968.
Walters, F. S., Slatin, S. L., Kulesza, C. A. & English, L. H. (1993). *Biochem. Biophys. Res. Commun.* **196**, 921–926.
Wang, B.-C. (1985). *Methods Enzymol.* **115**, 90–111.
Wu, D. & Aronson, A. I. (1992). *J. Biol. Chem.* **267**, 2311–2317.
Wu, S.-J. & Dean, D. H. (1996). *J. Mol. Biol.* **255**, 628–640.